Compression Characterization of High-modulus Carbon Fibers

O. MONTAGNIER* AND CH. HOCHARD

Laboratoire de Mécanique et d'Acoustique, 31 chemin Joseph Aiguier
13402 Marseille Cedex 20, France

ABSTRACT : The study deals with testing and modeling the mesoscopic compression behavior of high-modulus carbon fibers-reinforced epoxy. These fibers are very stiff, but their compression performances are poor. To decrease the risk margins during the sizing process, it is necessary to determine their compression behavior as accurately as possible. Two tests were carried out on two types of high-modulus carbon fibers (M55J fibers and K63712 fibers): the pure compression Celanese test, which gives poor strain results, and a new pure bending test, which allows large displacements and generates higher strain levels. This bending test makes it possible to know without inverse calculation the load for any sections and to use machine specimens in order to avoid tab effects. An elastic nonlinear model (a power function of the strain) is proposed to describe the loss of compressive rigidity until the brittle rupture. Model coefficients are identified for the two materials with a simple inverse calculation. The pure bending test brought to light a highly nonlinear behavior of the unidirectional K63712 fibers.

KEY WORDS: compressive strength, failure strain, high-modulus carbon fiber, pure bending.

INTRODUCTION

High modulus carbon fibers, such as Dialead fibers, are very stiff. A quasi-isotropic ([0°,90°,45°,-45°]$_S$) material reinforced with these unidirectional fibers is twice as stiff as aluminum although its density is 1.6 times lower. Our studies on high-speed drive shafts have shown the great potential of these fibers [1,2]. Hollow laminated composite drive shafts (thin-walled tubes) are subjected to dynamic loading and torsional buckling forces. In the case of a subcritical drive shaft, the first critical speed (which is given in a first approximation by Equation (1)) must not be reached, and this structure must therefore be both stiff along the rotational axis and lightweight.

$$f = \frac{\pi^2}{L^2}\sqrt{\frac{EI}{\rho S}} \tag{1}$$

where I is the bending moment of inertia, S the tube section surface, E the modulus along tube axis, L the tube length and ρ the material density.

Likewise, the torsional buckling critical load, which is one of the main criteria used in designing composite drive shafts, increases when the material has a high level of stiffness. However, these materials show a weakness for their compression properties.

To decrease the risk margins during the sizing of these structures, a very good knowledge of the

* Author to whom correspondence should be sent.
E-mail: oliviermontagnier@yahoo.fr ; phone: 33(0)4-91-11-38-15

compressive behavior is necessary. The pure compression test is notoriously difficult and leads to premature failure: if the specimens are too long, they can break by buckling, and if they are too short, the edge effects are significant [3-12].

Many authors have attempted to minimize some of these difficulties by improving the compression test method [8-10] or by carrying out experiments of other kinds to measure the compressive strength and/or the compressive strain to rupture (in particular for high resistance carbon fibers). Pure compression tests on $[(\pm 60°)_2, 0°, (\pm 60°)_2]_s$ laminates have been developed, which limit the risk of buckling and decrease the tab effects [11,12]. The main difficulty with this method is how to determine the in-plane behavior of the material exactly in order to perform the inverse calculations. Wisnom has designed a pin-ended buckling rig [3-5]. The advantage of buckling tests is that failure occurs in these tests without any stress concentration. They yield direct measurements of the compressive strain and generate high levels of strain. However, buckling tests do not make it possible to directly determine the load in the beam and it is therefore necessary to perform an inverse calculation with beam theory for large displacements. The fact that the behavior of the material/beam under compression is nonlinear makes this inverse calculation all the more complex. Other authors have carried out four-point bending tests to determine the compression behavior. For thick composites, Daniel proposed a four point bending test with small displacements adapted to performing an inverse calculation [9]. For flexible structures like thin composites, the four point bending test is not adapted due to the complex computation of the bending moment in large displacements and rotations [6,13]. In addition, these tests led to premature failure due to the stress concentration occurring at the hinges.

In the present study, two tests were carried out on high-modulus carbon fibers to determine compression behavior (Mitsubishi Dialead® K63712 / Structil R367-2 and Toray M55J / Structil R368-1): a pure compression test and a new pure bending test in large displacements. A nonlinear model is proposed to describe the loss of rigidity occurring under compression loading. The compression behavior identification method starting with pure bending tests is presented and applied to the two materials. The failure mode involved in the two unidirectional cases under investigation will also be discussed. Lastly, the two types of high-modulus carbon fibers, M55J fibers obtained from a PAN precursor and Dialead K63712 fibers obtained from PITCH, are compared.

PURE COMPRESSION TEST

Pure compression tests were performed with the Celanese test fixture (ASTM D3410) composed of two male prisms and two female prisms guided by a circular envelope (Figure 1). Only the Dialead K63712 unidirectional was studied to compare to the pure bending test. Six specimens were machined (Figure 1). Four specimens were equipped with a strain gauge on one face, while the other two were equipped with a strain gauge on each face. The tabs were cut out from a plate of [±45°]s CFRP.

Results

In each test, the compressive failure strain ε_c and the failure stress (load/section) σ_c were noted and the coefficient of variation (*cov*) was calculated. The initial compression modulus E_c was identified on test specimens with two strain gauges (Table 1). One of the advantages of this test is that the stress calculation is independent of the behavior of the material. The results show great dispersion and the failure stresses are underestimated in comparison with the manufacturer's experimental data (Table 1). The curves obtained were nonlinear but the method is not accurate enough to be able to extract the nonlinear material parameters (Figure 2).

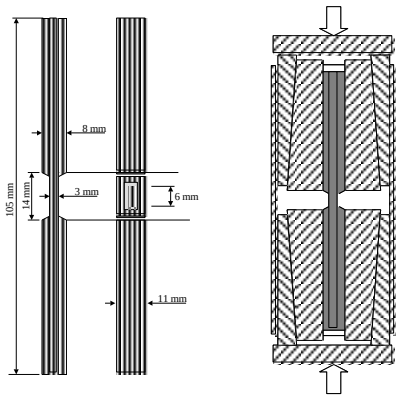

Figure 1. *Celanese specimens (carbon / epoxy tabs) and Celanese test fixture.*

Table 1. Mechanical characteristics of K63712 (normalized 60% volume fiber).

Parameter	Celanese test (Standard ASTM D3410)	Data
ε_c (*cov*)	0.10% (13.6%)	-
E_c	367 GPa	330[1] GPa
σ_c (*cov*)	374 MPa (5.1%)	440[1] MPa
E_T	-	370[2] GPa
σ_t	-	1500[2] MPa

[1] Mitsubishi (standard ASTM D695), [2] Mitsubishi.

Table 2. Mechanical characteristics of M55J (normalized 60% volume fiber).

Parameter	Celanese test (Standard ASTM D3410)	Data
σ_c	-	880[1] MPa
E_T	-	311 - 335[2] ; 338[1] GPa
σ_t	-	1760[3] ; 2010[1] MPa
ε_t	-	0,53[3] ; 0,6[1] %

[1] Torayca, [2] initial tangent modulus and final secant modulus [17], [3] [17]

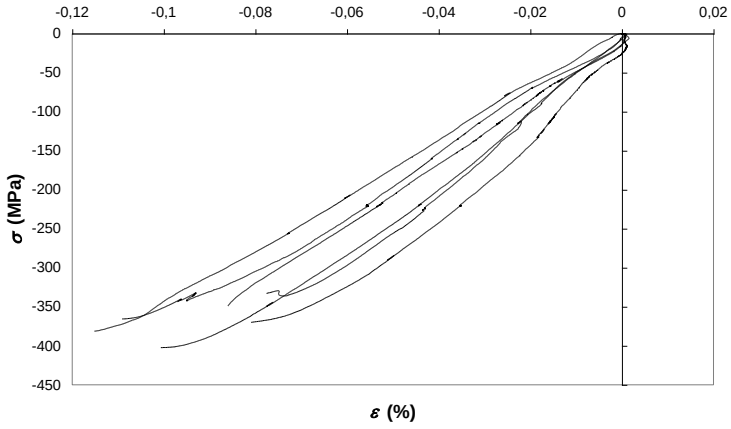

Figure 2. *Six Celanese compression test on K63712 (normalized 60% volume fiber).*

Analysis

The authors noted several points, like many others, that do not confirm the validity of the present experimental results [3-12]. First, in the specimens with two strain gauges, the difference between the strains was sometimes highly significant, which suggests that significant parasite bending may have occurred. Secondly, the assumption that there was a uniform strain field under the gauge is not valid because the free area on the specimen was too small. Thirdly, failure was observed systematically at the tabs due to the clamp and the rupture presumably occurred at an earlier stage. Fourthly, specimen-machining defects such as the lack of parallelism of the tabs can generate parasitic loads due to the high level of hyperstatism.

This test is therefore not a proper material test because it involves significant structural effects. More satisfactory results would certainly be obtained by performing a larger number of tests and eliminating those where the bending is too significant.

The manufacturer's experimental data on M55J unidirectional ply laminates are given in Table 2.

PURE BENDING TEST

A pure bending test is propose that allows large displacements. The principle on which the apparatus used for this purpose was based is quite simple (Figure 3-4). Four pulleys were assembled on the two axis of application of the bending moment and bearings were mounted at the axle ends. One axle was free to perform rotations but not displacements, and the other was free to perform both rotations and displacements. The bending moment was introduced by applying equal loads to each scale. The simplicity of the apparatus makes it possible to rule out the occurrence of any parasitic loads except for rolling friction, which will be neglected here. The specimens were machined in order to avoid tab effects (Figure 5). With this bending test, a specimen with a variable section does not introduce any analytical problems. The specimens were equipped with strain gauges on each face. The small section variation allows to assume a uniform strain field under the gauges. The test was carried out by applying several load increments.

Other kind of pure bending bench can be found in the literature. For steel beam, authors proposed to use four pulleys blocked in displacement on the other hand the beam is free to move along the contact rollers [14-16]. Recently, Zineb proposed a pure bending test with large displacements and rotations for composite structures where the bending moment is obtained with a simple inverse calculation independent of the specimen behavior [13].

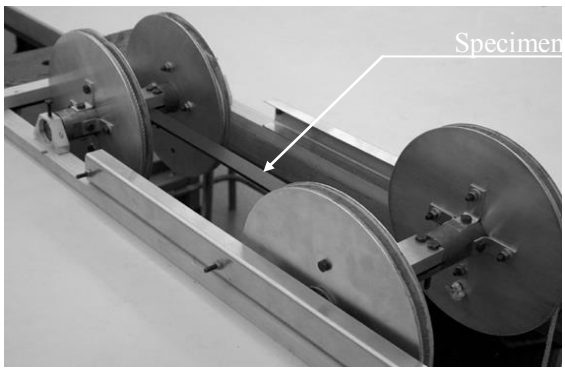

Figure 3. *Pure bending test apparatus.*

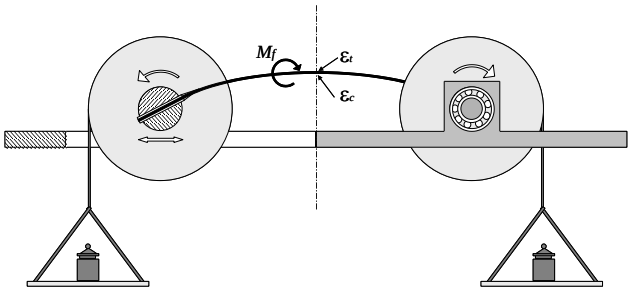

Figure 4. *Scheme of pure bending test apparatus.*

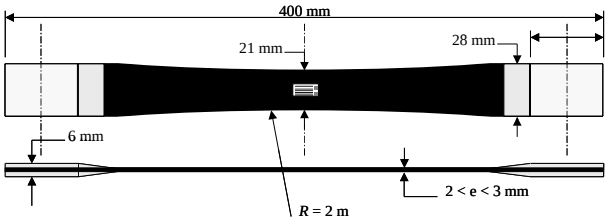

Figure 5. *Pure bending test specimen.*

Four specimens on each of the two materials were tested. The thickness was 2.22mm (20 plies) for the M55J unidirectional and 2.56mm (10 plies) for the K63712 unidirectional. It should be noted that Wisnom observed that the strain gradient through the thickness is a critical parameter [4,5]. The compressive strain at failure increased with the increase of the strain gradient. Buckling tests on T800/924 carbon fiber/epoxy showed a significant structural effect with thin specimens (mainly with a thickness inferior to 3mm).; The strain at failure of these high resistance fibers is superior to 1.5%, which involves a significant curvature for thin specimens. For high-modulus fibers, the strain at failure is inferior to 0.3%, which involves weak curvature in flexural tests with specimens of a 2.2mm thickness. This curvature corresponds to a T800/924 specimen thickness of 11mm. Hence, the strain gradient effect seems to be negligible here.

Results

The failure occurred in the middle of the specimen and the stresses concentrating at the clamps were not responsible for the failure. These tests yielded high failure strains with both materials (Figures 6 and 7). For the K63712, the strain at failure is about 60% greater than that obtained in the Celanese test (Table 3). For the two materials, tests were reproducible. The coefficient of variation of the compressive strain at failure is lower than 5%. The present results show the occurrence of non-linearly decreasing compression behavior. It is worth noting that the decrease in the tension strain does not mean that the tension behavior was a non-linearly decreasing behavior: it simply reflected the evolution of the equilibrium. To model the tension behavior, it will be necessary to carry out tension tests.

The failure mode was found to differ between the two materials. In the case of the M55J specimens, the failure was brittle (Figure 6), whereas in the case of the Dialead specimens, the failure mode was an original one. After point A had been reached (Figure 7), the strains increased slowly under a constant bending moment: during the first 85 seconds, the compressive strain evolved from 0.18% to 0.40%, the tensile strain evolved from 0.16% to 0.27%, and the neutral fiber moved

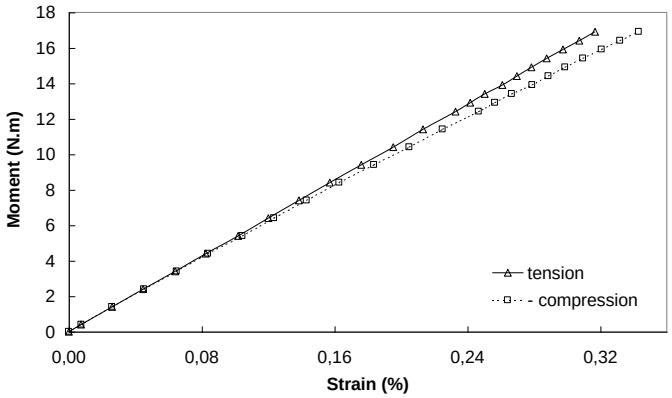

Figure 6. *A pure bending test on M55J until failure.*

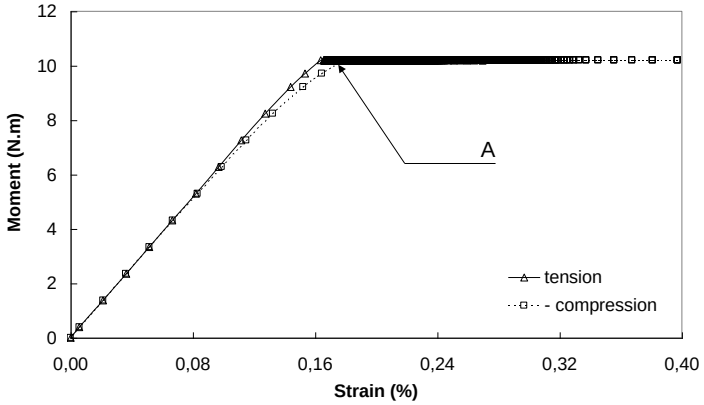

Figure 7. *A pure bending test on K63712 until failure.*

Table 3. Compressive failure strain of M55J and K63712 in pure bending tests

Material	Parameter	Identification
M55J	ε_c (*cov*)	0.311% (4.6%)
K63712	ε_c^A (*cov*)	0.168% (4.3%)

towards the tension zone.

Contrary to what was done in the case of the pure compression test, the failure stress was obtained starting with a mathematical model for the constitutive law. In the case of materials with linear behavior, the behavior can be determined quite straightforwardly because the bending moment is a linear function of the curvature. In the case of materials with nonlinear behavior, the inverse calculation is more complex.

Modelling and identification

The idea on which this study was based was to use mesoscopic models to describe the compression behavior of unidirectional plies, with a view to introduce these models into structural computations. This model is not based on microscopic processes such as fiber microbuckling, where

the homogenization procedure is highly complex.

In addition, the identification of the compression behavior based on the pure bending tests requires the tension behavior of the material to be known. Moreover, an increase in the stiffness has been observed during tensile tests on unidirectional M55J/M18 [17] (Table 2), where the secant modulus increased from 311 GPa to 335 Gpa [17]. Accordingly, tensile tests were carried out and a simple model was introduced to describe the nonlinear tension behavior.

TENSION BEHAVIOR: MODELLING AND IDENTIFICATION

Four tensile tests were carried out on each of the two materials (Figure 8). The tests showed the previously reported increase in the stiffness. This nonlinear behavior was modeled on a second-order power law:

$$\sigma_{11}=E_1\varepsilon_{11}+\beta<\varepsilon_{11}>_+^2 \tag{2}$$

where β is the nonlinear tensile parameter and $<\bullet>_+$ the positive part.

The results of these tests are presented in Table 4.

COMPRESSION BEHAVIOR: MODELLING

A mesoscopic model has been proposed by Ladevèze to model the compression behavior [18]. The decrease in the modulus was assumed here to be proportional to the stress, and the constitutive law was written:

$$\sigma_{11}=E_1\varepsilon_{11}-\alpha<\sigma_{11}>_-\varepsilon_{11} \tag{3}$$

where α is the nonlinear compressive parameter and $<\bullet>_-$ the negative part.

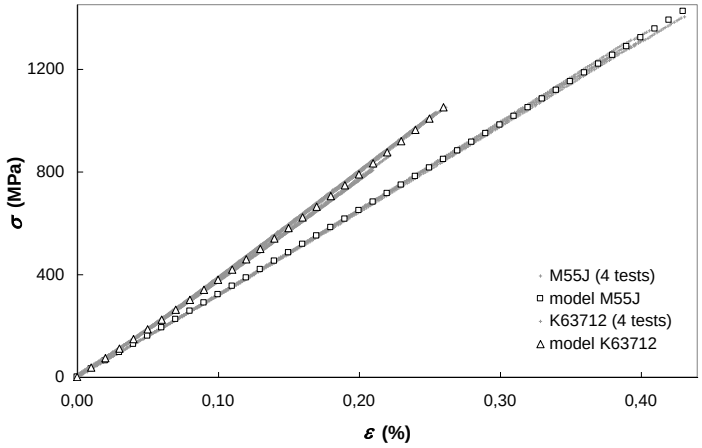

Figure 8. *Tensile tests and models for K63712 and M55J*

This model (written in terms of strain) was studied in the case of the two materials, but it does not satisfactorily describe the fast decrease in the compressive modulus that occurred in the Dialead unidirectional ply laminate at the end of the test (Figure 7). Another model with a different slope at the origin between tension and compression is also possible [6], but this assumption was not observed experimentally and seems to be less in keeping with physical reality. The authors therefore felt that it was logical to introduce a model where the decrease in the stiffness is taken to be proportional to a power function of the strain. After adding the tension behavior, the constitutive law becomes:

Table 4. Constitutive law parameters of M55J and K63712 identified by tensile tests (normalized 60% volume fiber).

Material	Parameter	Identification
M55J	E_1	318 Gpa
	β	308E3 GPa
K63712	E_1	363 Gpa
	β	1.58E4 GPa

$$\sigma_{11}=E_1\varepsilon_{11}-\alpha<-\varepsilon_{11}>_+^{n+1}+\beta<\varepsilon_{11}>_+^{2} \tag{4}$$

where n is the power of the power function.

Since parameters E_1 and β are defined by the results of the tensile tests, this law contains only two parameters which need to be determined, which are α and n.

COMPRESSION BEHAVIOR: IDENTIFICATION METHOD

The identification of α and n can be carried out point by point, but this does not suffice. The whole set of experimental data must be used to determine the parameters of the compressive constitutive law. Therefore a minimization method similar to that proposed by Vittecoq is used [6]. The minimization was carried out on parameter α by taking the exponent n, which minimizes the error, in the set {0.1 ; 0.2 ; … ; 3}.

In the case of the pure bending test, the functional which has to be minimized is:

$$f=\sum_{k=1}^{m}\left[qN_{\_\mathrm{comp}}(k)^2+(1-q)(M_{f\_\mathrm{comp}}(k)-M_{f\_\mathrm{exp}}(k))^2\right] \tag{5}$$

where $q\in[0,1]$ is the balance factor and m the number of experimental values, the values computed are noted 'comp' and the experimental values are noted 'exp'.

To determine the functional, the beam cross-section equilibrium is written as:

$$N_{\_\mathrm{comp}}=b\int_{-h/2}^{h/2}\sigma_{11}(y)dy \tag{6}$$

$$M_{f\_\mathrm{comp}}=b\int_{-h/2}^{h/2}\sigma_{11}(y)ydy \tag{7}$$

where the stress σ_{11} is deduced from the constitutive law (Equation (4)). We separate the integrals from sets [*-h/2*, *d*] (compression part) and [*d*, *-h/2*] (tension part). Assuming the strain gradient to be linear along the thickness direction,

$$\varepsilon_{11}(y)=\gamma(y-d) \tag{8}$$

where d is the neutral line displacement and γ the curvature.

The neutral line displacement and the curvature are obtained from the experimental values:

$$d=\left(\frac{h}{2}+e\right)\left(\frac{\varepsilon_c^{\exp}+\varepsilon_t^{\exp}}{\varepsilon_c^{\exp}-\varepsilon_t^{\exp}}\right) \tag{9}$$

$$\gamma=\frac{\varepsilon_t^{\exp}-\varepsilon_c^{\exp}}{h+2e} \tag{10}$$

where h is the specimen thickness and e the gauge support thickness plus the adhesive film thickness ($e \approx 0.04$ mm).

Therefore

$$N_{\_comp}=a_N+b_N\alpha \quad ; \quad M_{f\_comp}=a_M+b_M\alpha \tag{11}$$

with

$$a_N=b\gamma E_1\left[-dh+\frac{\beta\gamma}{3}\left(\frac{h}{2}-d\right)^3\right] \quad ; \quad b_N=-b\frac{\gamma^{n+1}}{n+2}\left(\frac{h}{2}+d\right)^{n+2}E_1 \tag{12}$$

$$a_M=b\gamma E_1\left[\frac{h^3}{12}+\frac{\beta\gamma}{12}\left(\frac{3h}{2}+d\right)\left(\frac{h}{2}-d\right)^3\right] \quad ; \quad b_M=b\frac{\gamma^{n+1}}{n+2}\left(\frac{h}{2}-\frac{d+h/2}{n+3}\right)\left(\frac{h}{2}+d\right)^{n+2}E_1 \tag{13}$$

Since the functional has been determined, it now suffices to solve a linear system with one equation (n being selected from the previously defined set):

$$\frac{\partial f}{\partial \alpha}=0 \tag{14}$$

i.e.

$$\alpha=\frac{\sum_{k=1}^{m}(1-q)b_M(k)M_{f\_\exp}(k)-\sum_{k=1}^{m}(qa_N(k)b_N(k)h^2+(1-q)a_M(k)b_M(k))}{\sum_{k=1}^{m}(qb_N(k)^2h^2+(1-q)b_M(k)^2)} \tag{15}$$

The balance factor q is chosen so as to minimize the average error in the normal force and the bending moment:

$$e_{\_N}=\frac{1}{m}\sqrt{\sum_{k=1}^{m}N_{\_comp}(k)^2} \tag{16}$$

$$e_{\_Mf}=\frac{1}{m}\sqrt{\sum_{k=1}^{m}(M_{f\_comp}(k)-M_{f\_\exp}(k))^2} \tag{17}$$

It is noted that the four specimens (denoted i) used for the pure bending tests differed in their sections and fiber volume fractions. To use the whole set of values in the minimization procedure, an equivalent bending moment is introduced:

$$M_{f\_\exp}(k)=\left(\frac{h^i}{2I_y^i}\right)\Big/\left(\frac{h^{\mathrm{ref}}}{2I_y^{\mathrm{ref}}}\right)M_{f\_\exp}{}^i(k)\frac{0.6}{V_f{}^i} \qquad \text{for} \quad i\in[1,...4]\,;\ k\in[1,...m] \tag{18}$$

where $I^i{}_y$ is the moment of inertia and $V^i{}_f$ the fiber volume fraction of a specimen i; the reference specimen is noted ‘ref’.

The maximum compressive stress σ_c was then computed starting with the model.

COMPRESSION BEHAVIOR: IDENTIFICATION

The model for the two materials with the optimum power (Equation (4)) is identified. The parameters identified are presented in Table 5.

Table 5. Constitutive law parameters of M55J and K63712 identified by pure bending tests (normalized 60% volume fiber).

Material	Parameter	Identification
M55J	*n*	0.2
	α (minimization error)	-85.0 GPa (0.0143 N.m)
	σ_c	906 MPa
K63712	*n*	2
	α (minimization error)	-3.52E7 GPa (0.0089 N.m)
	σ_c^A	443 MPa

To account for the variations in the section and fiber volume fraction in the model plot, the experimental moment is replaced by an equivalent stress (with a stress gradient assumed to be linear in the thickness):

$$\sigma_{equiv}(k)=\frac{h^i}{2I_y^i}\,M_{f\_\exp}{}^i(k)\frac{0.6}{V_f^i} \qquad \text{for} \quad i\in[1,...4];\ k\in[1,...m] \tag{19}$$

This equivalent stress does not have any physical significance in the case of nonlinear materials.

In addition, the measured strain has to be corrected to allow for the gauge support thickness and adhesive film thickness:

$$\varepsilon_c=\frac{-h/2+d}{-h/2+d+e}\varepsilon_c^{\exp} \tag{20}$$

$$\varepsilon_t=\frac{h/2-d}{h/2-d+e}\varepsilon_t^{\exp} \tag{21}$$

Starting from these definitions, the optimum models and the experimental values were plotted (Figures 9 and 10). The constitutive law was plotted for the two materials (Figures 11 and 12). In the case of the Dialead fibers, the power n=2 shows highly nonlinear behavior.

Analysis of the observed Dialead pure bending rupture

This pure bending test brought to light a failure mode with loss of stiffness for load controlled in the unidirectional K63712 (Figure 7). The strains increased in a relatively stable way with a constant load. Let us recall the failure was catastrophic on the unidirectional M55J (Figure 6). As a rule, compression failure is catastrophic for load controlled and even for displacement controlled. Vogler presented a complex experimental procedure to control the initiation and growth of kink bands in uniaxial composites [19,20]. Two explanations can be found for this effect.

The first is to say (Figure 7, point A) that a local failure or several local failures are occurring and propagating in a controlled way through the thickness of the specimen. After point A (Figure 13a), the local failure grows slowly and a new equilibrium appears (Figure 13b). According to several authors, the fiber microbukling initiation and propagation is matrix-dominated. The slow rate of propagation must have been due to the viscous processes occurring in the epoxy.

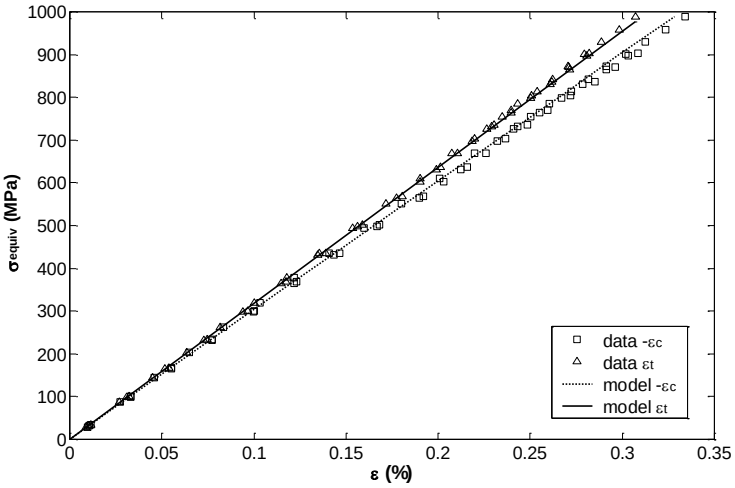

Figure 9. *M55J pure bending tests and models.*

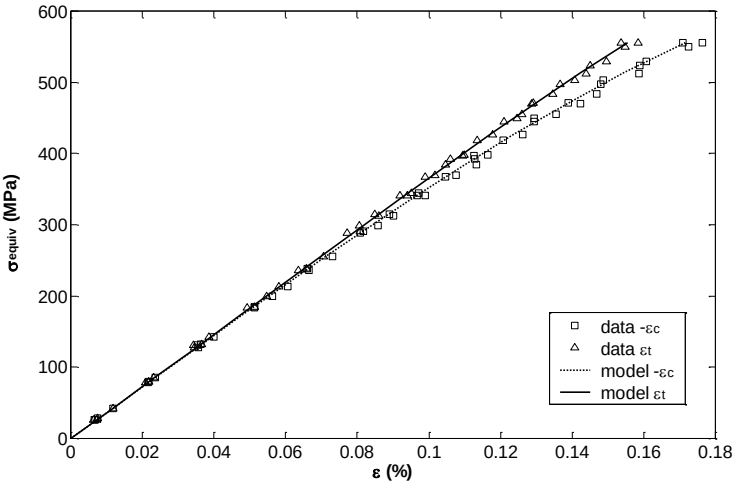

Figure 10. *K63712 pure bending tests and models.*

A second is that the relative stable propagation was due to the Dialead constitutive law (Figure 12) where point A (Figure 7) seems to coincide locally with the top of the compressive stress/strain curve. From this loading level onwards, the maximum compressive stress was reached (Figure 14a), the local behavior decreased and a new equilibrium appeared (Figure 14b). Again, the viscous processes occurring in the epoxy can explain the slow rate of propagation.

The best way to describe the stable propagation of the compression failure is microscopic analysis. In this framework of structure computation, our objective was to model the behavior of complex structures until the rupture of the first ply (conservative approach). The model has to be as simple as possible and hence this rupture phenomenon is not taken into account in this model.

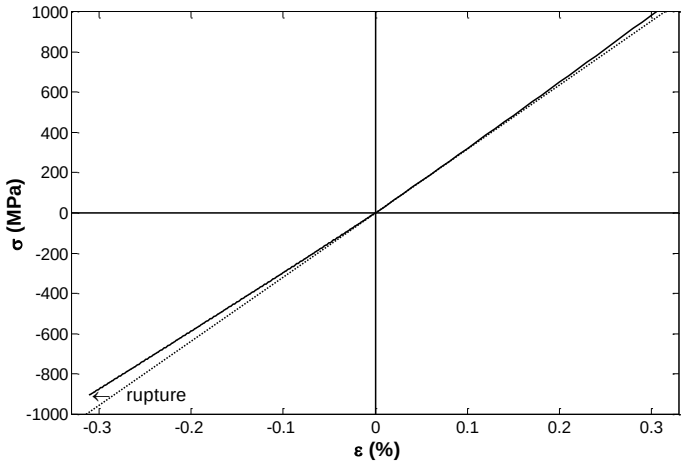

Figure 11. *M55J constitutive law in the fiber direction.*

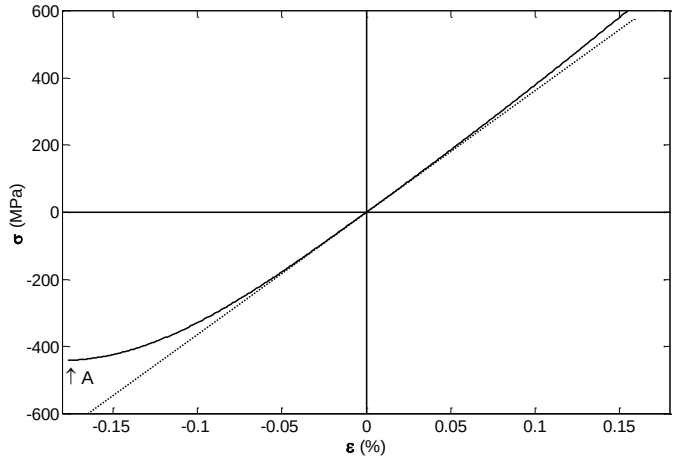

Fig. 12. *K63712 constitutive law in the fiber direction.*

COMPARISON BETWEEN HIGH-MODULUS FIBERS

Pitch-based carbon fibers are much less expensive than high-modulus PAN-based fibers. The first point worth mentioning here is that M55J fibers are stronger, and that the difference between the two materials is greater under compression than under tension loading. The compression failure stress is approximately only half of the tension failure stress in the case of M55J fibers and only one third in the case of K63712 fibers. The initial stiffness of the M55J is slightly lower (12%), but there is a much greater loss of stiffness under compression in the case of K63712 fibers. Lastly, the density of the composite is greater in the case of K63712 (2.12 as against 1.91 in the case of M55J).

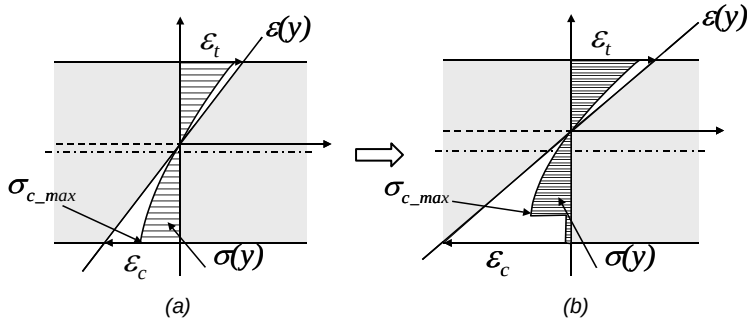

Figure 13. *Local equilibrium evolution for a constant bending moment in the K63712 specimens: brittle rupture.*

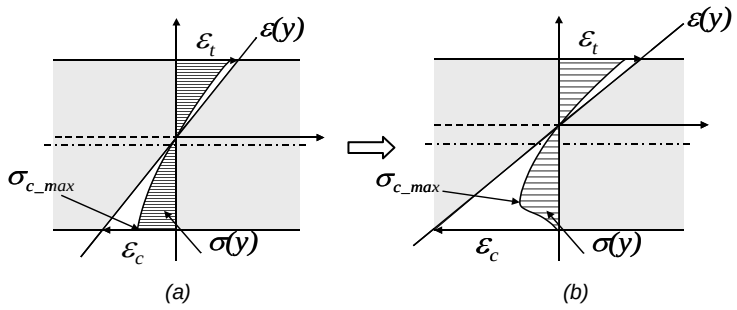

Figure 14. *Local equilibrium evolution for a constant bending moment in the K63712 specimens: progressive rupture.*

CONCLUSION

The Celanese pure compression test leads to premature ruptures in high-modulus carbon fibers. The pure bending test proposed here makes it possible to define the compression behavior even in large displacements. A nonlinear model (a power function of the strain) is proposed and a local inverse calculation is required for the identification. The very low compressive strain at failure of high-modulus fibers and highly nonlinear behavior of Dialead are highlighted. These tests showed the occurrence of brittle rupture in the M55J unidirectional ply laminates and an unusual rupture process in the Dialead unidirectional ply laminates.

The existence of this non-linearity has significant implications for drive shaft design, especially as regards the use of Dialead fibers. Firstly, because of the decrease of the modulus, torsional buckling computations on these materials with linear behavior tend to overestimate the critical load. Secondly, for a better sizing of laminates up to rupture, the nonlinear elastic behavior has to be taken into account.

REFERENCES

1. Montagnier, O. and Hochard, Ch. (2003). Dimensionnement de tubes composites à haute vitesse de rotation, In: *Proceedings of the 16ème Congrès Français de Mécanique*, Nice, France.

2. Montagnier, O. and Hochard, Ch. (2004). Design of high rotation frequency composite tubes, In: *Proceedings of the 11th European Conference on Composite Materials*, Rhodes, Greece.

3. Wisnom, M.R. (1992). On the high compressive strains achieved in bending tests on unidirectional carbon-fiber/epoxy, *Composites science and technology*, **43**: 229-235.

4. Wisnom, M.R. and Atkinson J.W. (1997). Constrained buckling tests show increasing compressive strain to failure with increasing strain gradient, *Composites Part A*, **28A**: 959-964.
5. Wisnom, M.R. (1999). Size effects in the testing of fibre-composite materials, *Composites science and technology*, **59**: 1937-1957.
6. Vittecoq, E. (1991). Comparison between compression and tension behaviors of composite laminates, Thesis, Paris 6.
7. Woolstencroft, D.H. Curtis, A.R. and Haresceugh R.I. (1981). A comparison of test techniques used for evaluation of unidirectional compressive strength of carbon fiber-reinforced plastic, *Composites* **12**(4): 275-280.
8. Daniel, I.M. Hsiao, H-M. Wooh, S-C. and Vittoser, J. (1993). In: *Processing and compressive behavior of thick composites*, AMD-Vol.162 Mechanism of Thick Composites, ASME: 107-126.
9. Daniel, I.M. Hsiao, H-M. and Wooh, S-C. (1996). Failure mechanisms in thick composites under compressive loading, *Composites Part B*, **27B**: 543-552.
10. Daniel, I.M. and Hsiao, H-M. (1999). Is there thickness effect on compressive strength of unnotched composite laminates, *International journal of fracture*, **95**: 143-158.
11. Anquez, L. (1994). Experimental investigations to assess typical compressive behavior of composites, In: *Proceedings of the 30th Polymer Matrix Composites Coordination Group Meeting* (MIL-HDBK-17), New Orleans, L.A.: 139-146.
12. Welsh, J.S. and Adams, D.F. (1997). Testing of angle-ply laminates to obtain unidirectional composite compression strengths, *Composites Part A*, **28**: 387-396.
13. Zineb, T.B. Sedrakian, A. and Billoet, J.L. (2003). An original pure bending device with large displacements and rotations for static and fatigue tests of composite structures, *Composites Part B*, **34B**: 447-448.
14. Elchalakani M. Zhao, X.L. and Grzebieta, R.H. (2001). Concrete-filled circular steel tubes subjected to pure bending, *Journal of Constructional Steel Research*, **57**: 1141-1168.
15. Aguirre, F. Kyraikydes, S. and Yun, H.D. (2004). Bending of steel tubes with Lüders bands, *International Journal of Plasticity*, **34B**: 447-448.
16. Ellison, M.S. and Corona, E. (1998). Buckling of T-beams under cyclic bending, *International Journal of Mechanical Sciences*, **40(9)**: 835-855.
17. Lévêque, D. (1998). Analyse de la tenue au délaminage des composites stratifiés: identification d'un modèle d'interface interlaminaire, Thesis, Ecole Normale Supérieure de Cachan.
18. Ladevèze, P. (1992). A damage computational method for composite structures, *Computers & Structures*, **44**: 79-87.
19. Vogler, T.J. and Kyraikydes, S. (1997). Initiation and axial propagation of kink bands in fiber composites, *Acta Materialia*, **45(6)**: 2443-2454.
20. Vogler, T.J. and Kyraikydes, S. (2001). On the initiation and growth of kink bands in fiber composites: Part I. experiments, *International Journal of Solids and Structures*, **38**: 2639-2651.